

## Search for Very Light $CP$ -Odd Higgs Boson in Radiative Decays of $\Upsilon(1S)$

W. Love,<sup>1</sup> V. Savinov,<sup>1</sup> H. Mendez,<sup>2</sup> J. Y. Ge,<sup>3</sup> D. H. Miller,<sup>3</sup> I. P. J. Shipsey,<sup>3</sup> B. Xin,<sup>3</sup> G. S. Adams,<sup>4</sup> M. Anderson,<sup>4</sup> J. P. Cummings,<sup>4</sup> I. Danko,<sup>4</sup> D. Hu,<sup>4</sup> B. Moziak,<sup>4</sup> J. Napolitano,<sup>4</sup> Q. He,<sup>5</sup> J. Insler,<sup>5</sup> H. Muramatsu,<sup>5</sup> C. S. Park,<sup>5</sup> E. H. Thorndike,<sup>5</sup> F. Yang,<sup>5</sup> M. Artuso,<sup>6</sup> S. Blusk,<sup>6</sup> S. Khalil,<sup>6</sup> J. Li,<sup>6</sup> R. Mountain,<sup>6</sup> S. Nisar,<sup>6</sup> K. Randrianarivony,<sup>6</sup> N. Sultana,<sup>6</sup> T. Skwarnicki,<sup>6</sup> S. Stone,<sup>6</sup> J. C. Wang,<sup>6</sup> L. M. Zhang,<sup>6</sup> G. Bonvicini,<sup>7</sup> D. Cinabro,<sup>7</sup> M. Dubrovin,<sup>7</sup> A. Lincoln,<sup>7</sup> P. Naik,<sup>8</sup> J. Rademacker,<sup>8</sup> D. M. Asner,<sup>9</sup> K. W. Edwards,<sup>9</sup> J. Reed,<sup>9</sup> R. A. Briere,<sup>10</sup> T. Ferguson,<sup>10</sup> G. Tatishvili,<sup>10</sup> H. Vogel,<sup>10</sup> M. E. Watkins,<sup>10</sup> J. L. Rosner,<sup>11</sup> J. P. Alexander,<sup>12</sup> D. G. Cassel,<sup>12</sup> J. E. Duboscq,<sup>12</sup> R. Ehrlich,<sup>12</sup> L. Fields,<sup>12</sup> R. S. Galik,<sup>12</sup> L. Gibbons,<sup>12</sup> R. Gray,<sup>12</sup> S. W. Gray,<sup>12</sup> D. L. Hartill,<sup>12</sup> B. K. Heltsley,<sup>12</sup> D. Hertz,<sup>12</sup> J. M. Hunt,<sup>12</sup> J. Kandaswamy,<sup>12</sup> D. L. Kreinick,<sup>12</sup> V. E. Kuznetsov,<sup>12</sup> J. Ledoux,<sup>12</sup> H. Mahlke-Krüger,<sup>12</sup> D. Mohapatra,<sup>12</sup> P. U. E. Onyisi,<sup>12</sup> J. R. Patterson,<sup>12</sup> D. Peterson,<sup>12</sup> D. Riley,<sup>12</sup> A. Ryd,<sup>12</sup> A. J. Sadoff,<sup>12</sup> X. Shi,<sup>12</sup> S. Stroiney,<sup>12</sup> W. M. Sun,<sup>12</sup> T. Wilksen,<sup>12</sup> S. B. Athar,<sup>13</sup> R. Patel,<sup>13</sup> J. Yelton,<sup>13</sup> P. Rubin,<sup>14</sup> B. I. Eisenstein,<sup>15</sup> I. Karliner,<sup>15</sup> S. Mehrabyan,<sup>15</sup> N. Lowrey,<sup>15</sup> M. Selen,<sup>15</sup> E. J. White,<sup>15</sup> J. Wiss,<sup>15</sup> R. E. Mitchell,<sup>16</sup> M. R. Shepherd,<sup>16</sup> D. Besson,<sup>17</sup> T. K. Pedlar,<sup>18</sup> D. Cronin-Hennessy,<sup>19</sup> K. Y. Gao,<sup>19</sup> J. Hietala,<sup>19</sup> Y. Kubota,<sup>19</sup> T. Klein,<sup>19</sup> B. W. Lang,<sup>19</sup> R. Poling,<sup>19</sup> A. W. Scott,<sup>19</sup> P. Zweber,<sup>19</sup> S. Dobbs,<sup>20</sup> Z. Metreveli,<sup>20</sup> K. K. Seth,<sup>20</sup> A. Tomaradze,<sup>20</sup> J. Libby,<sup>21</sup> L. Martin,<sup>21</sup> A. Powell,<sup>21</sup> G. Wilkinson,<sup>21</sup> and K. M. Ecklund<sup>22</sup>

(CLEO Collaboration)

<sup>1</sup>University of Pittsburgh, Pittsburgh, Pennsylvania 15260, USA

<sup>2</sup>University of Puerto Rico, Mayaguez, Puerto Rico 00681

<sup>3</sup>Purdue University, West Lafayette, Indiana 47907, USA

<sup>4</sup>Rensselaer Polytechnic Institute, Troy, New York 12180, USA

<sup>5</sup>University of Rochester, Rochester, New York 14627, USA

<sup>6</sup>Syracuse University, Syracuse, New York 13244, USA

<sup>7</sup>Wayne State University, Detroit, Michigan 48202, USA

<sup>8</sup>University of Bristol, Bristol BS8 1TL, United Kingdom

<sup>9</sup>Carleton University, Ottawa, Ontario, K1S 5B6 Canada

<sup>10</sup>Carnegie Mellon University, Pittsburgh, Pennsylvania 15213, USA

<sup>11</sup>Enrico Fermi Institute, University of Chicago, Chicago, Illinois 60637, USA

<sup>12</sup>Cornell University, Ithaca, New York 14853, USA

<sup>13</sup>University of Florida, Gainesville, Florida 32611, USA

<sup>14</sup>George Mason University, Fairfax, Virginia 22030, USA

<sup>15</sup>University of Illinois, Urbana-Champaign, Illinois 61801, USA

<sup>16</sup>Indiana University, Bloomington, Indiana 47405, USA

<sup>17</sup>University of Kansas, Lawrence, Kansas 66045, USA

<sup>18</sup>Luther College, Decorah, Iowa 52101, USA

<sup>19</sup>University of Minnesota, Minneapolis, Minnesota 55455, USA

<sup>20</sup>Northwestern University, Evanston, Illinois 60208, USA

<sup>21</sup>University of Oxford, Oxford OX1 3RH, United Kingdom

<sup>22</sup>State University of New York at Buffalo, Buffalo, New York 14260, USA

(Received 9 July 2008; published 10 October 2008)

We search for a non-SM-like  $CP$ -odd Higgs boson ( $a_1^0$ ) decaying to  $\tau^+\tau^-$  or  $\mu^+\mu^-$  in radiative decays of the  $\Upsilon(1S)$ . No significant signal is found, and upper limits on the product branching ratios are set. Our  $\tau^+\tau^-$  results are almost 2 orders of magnitude more stringent than previous upper limits. Our data provide no evidence for a Higgs state with a mass of 214 MeV decaying to  $\mu^+\mu^-$ , previously proposed as an explanation for 3  $\Sigma^+ \rightarrow p\mu^+\mu^-$  events observed by the HyperCP experiment. Our results constrain NMSSM models.

DOI: [10.1103/PhysRevLett.101.151802](https://doi.org/10.1103/PhysRevLett.101.151802)

PACS numbers: 14.80.Cp, 11.30.Pb, 12.60.Fr, 13.20.Gd

Direct searches at LEP for the Standard Model Higgs boson, a  $CP$ -even scalar, set a lower bound on its mass in excess of  $10^2$  GeV [1]. Many extensions of the Standard Model predict the existence of a  $CP$ -odd pseudoscalar

Higgs boson (hereafter, denoted as  $a_1^0$ ), which could be light. For example, the Next-to-Minimal Super-Symmetric Model (NMSSM) with  $a_1^0$  mass below the threshold for  $a_1^0 \rightarrow b\bar{b}$  decay is particularly well motivated [2].

Radiative production in  $Y(1S)$  decays,  $Y(1S) \rightarrow \gamma a_1^0$ , offers a unique experimental opportunity to search for such a state. The couplings of the Higgs to fermions are proportional to their masses, therefore enhanced with respect to lighter mesons. The expected rate [3] is

$$\frac{\mathcal{B}(Y(1S) \rightarrow \gamma a_1^0)}{\mathcal{B}(Y(1S) \rightarrow \mu^+ \mu^-)} = \frac{G_F m_b^2}{\sqrt{2} \pi \alpha} g_d^2 \left[ 1 - \left( \frac{m_{a_1^0}}{m_{Y(1S)}} \right)^2 \right] \mathcal{C},$$

where  $G_F$  is the Fermi constant,  $\alpha$  is the fine structure constant,  $g_d$  is the  $a_1^0$  coupling to the down-type fermions, and  $\mathcal{C}$  incorporates QCD and relativistic corrections. The coupling  $g_d \propto \tan\beta \cos\theta_A$ , where  $\tan\beta$  is the ratio of vacuum expectations for the two Higgs doublets, and  $\theta_A$  is the mixing angle between doublet and singlet  $CP$ -odd Higgs bosons;  $g_d$  depends on the detailed choice of SUSY parameters. For  $m_{a_1^0} < 2m_b$ , the decay  $a_1^0 \rightarrow \tau^+ \tau^-$  is expected to dominate, especially at large  $\tan\beta$ ,  $\mathcal{B}(a_1^0 \rightarrow \tau^+ \tau^-) \sim 0.9$  [2]. For  $m_{a_1^0} < 2m_\tau$ ,  $a_1^0 \rightarrow \mu^+ \mu^-$  decays are copious below the  $s\bar{s}$  threshold. In fact, it has been suggested that 3  $\Sigma^+ \rightarrow p\mu^+\mu^-$  events observed by the HyperCP experiment [4] are due to a  $CP$ -odd Higgs with a mass of  $214.3 \pm 0.5$  MeV [5].

The data for this search were acquired with the CLEO-III detector [6] operating at the Cornell Electron Storage Ring (CESR) and correspond to an integrated luminosity of  $1.1 \text{ fb}^{-1}$  at the  $Y(1S)$  resonance, yielding  $(21.5 \pm 0.4) \times 10^6$  resonant decays. We also use  $7 \text{ fb}^{-1}$  of data collected at and near the  $Y(4S)$  resonance for continuum background studies.

We select events with exactly two tracks of opposite charge and at least one  $\gamma$ . The highest energy  $\gamma$  passing  $\pi^0$  veto cut is selected to be a candidate for  $Y(1S) \rightarrow \gamma a_1^0$ . For optimal energy resolution and smallest backgrounds, the radiative-decay  $\gamma$  is required to be in the barrel part of the calorimeter ( $|\cos\theta| < 0.8$ ). Its lateral shower profile must be consistent with an isolated electromagnetic shower.

To select  $a_1^0 \rightarrow \tau^+ \tau^-$  candidates, we require a missing energy between 2 and 7 GeV. The total energy calculation is based on charged track momenta (the pion mass is assumed) and calorimeter energy for  $\gamma$  candidates. To suppress hadronic events from the continuum production and  $Y(1S)$  decays, at least one of the charged tracks must be identified as an electron or a muon. Events with two electrons are discarded to suppress Bhabha-like events, which are already mostly eliminated by the missing energy requirement. Besides being identified in the muon system, the  $\mu$  candidate is required to have an energy deposited in the calorimeter ( $E$ ) consistent with a minimum ionizing particle. The electron candidate must have  $E$  equal to  $p$  within  $\pm 15\%$ .  $dE/dx$  consistency is required for leptons. The invariant mass of photons (except for the radiative-decay  $\gamma$ ) plus the charged track not identified as a lepton is required to be less than 2 GeV. To suppress final state radiation, the cosine of the angle between any charged track and the  $\gamma$  candidate must be less than 0.99.

We search for evidence for a signal of a monochromatic peak in the  $\gamma$  energy distribution. Thus, our results assume that the  $a_1^0$  natural width is negligible compared with the experimental resolution, an assumption which is expected to be true, with the exception of the heaviest masses probed in the  $\tau^+ \tau^-$  channel, due to possible mixing with the  $\eta_b$  [7]. CLEO previously published an alternative method for probing the  $a_1^0$  mass approaching the  $b\bar{b}$  states, which is not sensitive to assumptions about its width [8].

The selected event sample is composed mostly of continuum  $e^+e^- \rightarrow (\gamma)\tau^+\tau^-$  events, where the  $\gamma$  candidate comes either from initial state radiation (ISR) or from a  $\pi^0$  produced in  $\tau$  decay, with the second  $\gamma$  not reconstructed. The background estimates are superimposed on top of the spectrum obtained at the  $Y(1S)$  resonance in Fig. 1(a). The continuum backgrounds are estimated by scaling the  $Y(4S)$  distributions. There is also a significant contribution from  $Y(1S) \rightarrow \tau^+ \tau^-$  with the  $\gamma$  candidate coming from a  $\pi^0$  decay. The observed  $\gamma$  spectrum with binning comparable to our  $\gamma$  energy resolution is shown in Fig. 1(c). No significant peaks are observed.

The channel  $a_1^0 \rightarrow \mu^+ \mu^-$  is selected by identifying both muons. We require that the total observed energy be within 250 MeV of the center-of-mass energy. The invariant di-

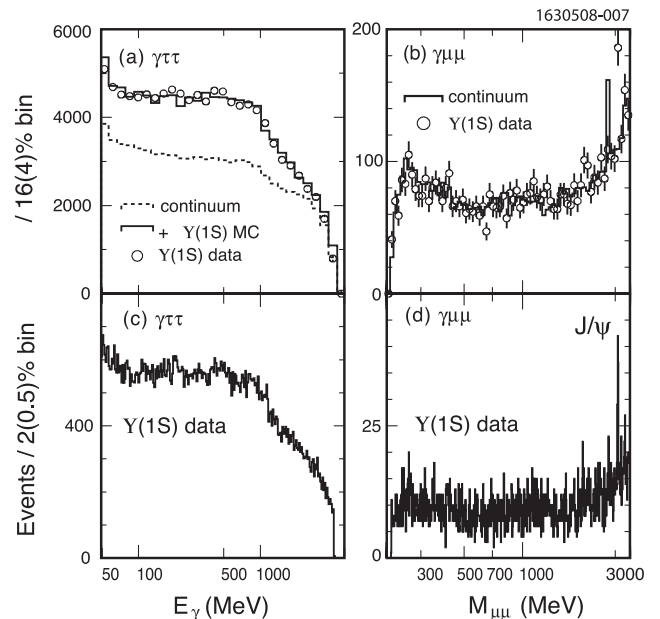


FIG. 1. Photon energy and dimuon mass distributions in  $\gamma\tau^+\tau^-$  (a), (c) and  $\gamma\mu^+\mu^-$  (b), (d) data, respectively. Bin size for the right column plots is given in the axes labels in parentheses. In the top row, the  $Y(1S)$  data (points with error bars) are compared to the estimated backgrounds (dashed and solid lines). In the bottom row, the  $Y(1S)$  data (solid line) are shown in fine binning comparable to the detector resolution (see bottom row of Fig. 2). In (b), the  $J/\psi$  ISR peak is shifted in the background estimate since we scaled  $\mu$  momenta down by the ratio of the beam energies when scaling the higher energy data to the  $Y(1S)$  distribution.

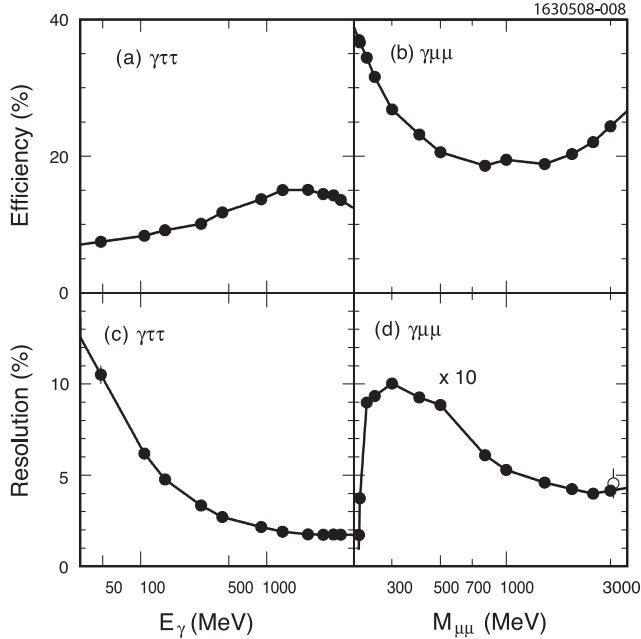


FIG. 2. Efficiency (a), (b) and  $a_1^0$  mass resolution (c), (d) obtained from the fits to the  $a_1^0 \rightarrow \tau^+\tau^-$  (left column) and  $a_1^0 \rightarrow \mu^+\mu^-$  (right column) signal MC (points) and interpolated for the regions in between (solid line). In (d), relative dimuon mass resolution was multiplied by a factor of 10. See Appendix C of Ref. [3] for explanation of improvement of the dimuon mass resolution near the kinematic threshold. The hollow point with the error bar in (d) represents the fit of the mass resolution to the  $J/\psi \rightarrow \mu^+\mu^-$  ISR peak observed in the  $Y(1S)$  data.

muon mass has better resolution than the  $\gamma$  energy; therefore, we use it to look for the  $a_1^0$  signal. The selected data are dominated by radiative  $\mu$ -pairs with a hard radiative photon. The data selected at the peak of the  $Y(1S)$  resonance are well described by scaling the data collected at and near the  $Y(4S)$  as illustrated in Fig. 1(b). The  $Y(1S)$  distribution plotted with binning comparable to our dimuon mass resolution is shown in Fig. 1(d). No significant peak is found except for the  $J/\psi$  produced by ISR.

The signal efficiency varies with Higgs mass, or equivalently,  $\gamma$  energy. In order to determine the efficiency, we generated signal Monte Carlo (MC) for several  $a_1^0$  masses and interpolated for masses in between. Proper angular correlations were implemented in the MC for both the polar angle of the radiative  $\gamma$  and for  $\tau$  polarizations [9]. The signal peaks observed in the dimuon mass ( $\gamma$  energy) distribution for  $a_1^0 \rightarrow \mu^+\mu^-$  ( $a_1^0 \rightarrow \tau^+\tau^-$ ) were fitted to a Gaussian (with an asymmetric low energy tail, i.e., a Crystal Ball line shape [10]) to determine reconstruction efficiency and detector resolution, which are shown in Figs. 2(a) and 2(c)(bd). The fit to the  $J/\psi \rightarrow \mu^+\mu^-$  ISR peak observed in the  $Y(1S)$  data gives a value for the resolution consistent with the MC expectations for an  $a_1^0 \rightarrow \mu^+\mu^-$  signal at that mass [Fig. 2(d)].

We have scanned the observed  $\gamma$  energy (50–4000 MeV) and dimuon mass (201–3565 MeV) distributions by fitting a signal peak on top of a cubic background polynomial, changing the peak position in steps equal to the detector resolution. The peak width was fixed to the MC expectations. The fit range was set to  $\pm 0.5$  of  $\ln(E_\gamma)$  [ $\pm 0.25$  of  $\ln(M_{\mu\mu})$ ] around the peak position. The  $J/\psi \rightarrow \mu^+\mu^-$  peak region was excluded within  $\pm 3\sigma$ , unless fitting a peak at the  $J/\psi$  mass. Since, in the dimuon channel, the continuum backgrounds saturate the  $Y(1S)$  sample [see Fig. 1(b)], we simultaneously fit the background polynomial to the dimuon mass distribution obtained from the higher statistics  $Y(4S)$  data. The overall background normalization factor for the  $Y(4S)$  data was included as a free parameter in the fit.

To test for possible bias in the fit procedure, we calculated average and root mean square (RMS) values of fitted signal amplitude ( $N$ ) divided by its error ( $\Delta N$ ). In absence of any signal peaks, values of 0.0 and 1.0 are expected, respectively. The average value for the data is  $+0.01 \pm 0.09$  ( $-0.06 \pm 0.05$ ) for the  $\gamma\tau^+\tau^-$  ( $\gamma\mu^+\mu^-$ ) sample, while the RMS is  $1.16 \pm 0.09$  ( $1.05 \pm 0.05$ ). To cover the observed deviations from the expectations, we assume 15% for a possible systematic error in the fit procedure.

The ratio of the fit likelihoods for a signal peak included in the fit ( $\mathcal{L}_{\max}$ ) and the data fit with the background term alone ( $\mathcal{L}_0$ ) is used to calculate the peak significance in standard deviations,  $\sqrt{2 \ln(\mathcal{L}_{\max}/\mathcal{L}_0)}$ . No peak with significance above  $3\sigma$  is found in the  $\gamma\tau^+\tau^-$  data. In the  $\gamma\mu^+\mu^-$  data, the ISR  $J/\psi$  peak has  $8.3\sigma$  significance. There are two other mass points which produce peaks with significance slightly above  $3\sigma$ :  $3.3\sigma$  at  $2041 \pm 4$  MeV and  $3.1\sigma$  at  $211.92 \pm 0.15$  MeV. For one trial, the probability ( $\epsilon$ ) of background fluctuations producing a peak with significance equal to or larger than  $3.3\sigma$  ( $3.1\sigma$ ) is 0.05% (0.1%). We performed 482 fits to  $\gamma\mu^+\mu^-$  spectrum with the peak positions separated by one unit of mass resolution. Assuming that peaks must be separated by at least 3 units of mass resolution to fluctuate independently, we performed about  $n = 482/3 \approx 160$  statistically independent trials. The overall probability in our scan of producing at least one peak with significance of at least  $3.3\sigma$  ( $3.1\sigma$ ) is  $1 - (1 - \epsilon)^n \approx 8\%$  (15%).

With no evidence for an  $a_1^0$  signal, we set upper limits on  $\mathcal{B}(Y(1S) \rightarrow \gamma a_1^0) \times \mathcal{B}(a_1^0 \rightarrow l^+l^-)$  ( $l = \tau$  or  $\mu$ ), which are displayed in Fig. 3. The limits were scaled up by 20% to account for the possible systematic error in the fit procedure (15%), in the efficiency calculation (MC statistics, interpolation between MC points, detector modeling; together  $< 10\%$ ), in number of  $Y(1S)$  decays (2%), and in simulation of detector resolution (10%). Our upper limits on  $\mathcal{B}(Y(1S) \rightarrow \gamma a_1^0) \times \mathcal{B}(a_1^0 \rightarrow \tau^+\tau^-)$  are almost 2 orders of magnitude more stringent than previously obtained by ARGUS [11]. Our upper limits on  $\mathcal{B}(Y(1S) \rightarrow \gamma a_1^0) \times \mathcal{B}(a_1^0 \rightarrow \mu^+\mu^-)$  are the first experimental bounds.

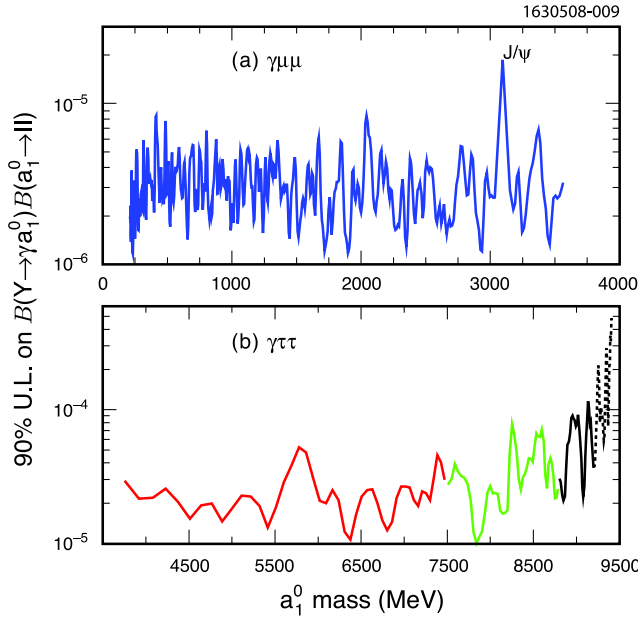


FIG. 3 (color online). Upper limits on  $\mathcal{B}(Y(1S) \rightarrow \gamma a_1^0)$  (a)  $\times \mathcal{B}(a_1^0 \rightarrow \mu^+ \mu^-)$  (b)  $\times \mathcal{B}(a_1^0 \rightarrow \tau^+ \tau^-)$  as a function of the  $a_1^0$  mass (90% C.L.). The gray coding [color coding online] corresponds to the one used in Fig. 4. The dashed line indicates the region ( $m_{a_1^0} > 9.2$  GeV) where  $a_1^0$  is likely to mix with  $\eta_b$  and acquire a non-negligible width, thus invalidating our analysis method.

Our  $\gamma\tau^+\tau^-$  results provide stringent constraints on NMSSM models, eliminating a large portion of previously unconstrained parameter space. This is illustrated in Fig. 4, where NMSSM calculations by Dermisek, Gunion, McElrath [2] are compared to our upper limits. While some model parameters were fixed (e.g.,  $\tan\beta = 10$ ) in the theoretical calculations, other parameters were sampled. Each point represents a different choice of NMSSM parameter values consistent with the current experimental constraints. The plot on the right represents models with the additional requirement of low fine-tuning of electroweak symmetry breaking (see Ref. [2] for details). Color coding corresponds to various  $a_1^0$  mass ranges. Our upper limits in various  $a_1^0$  mass ranges are shown by horizontal lines. Solid (dashed) line(s) represent an average (minimal and maximal) upper limits in given mass range. Assuming that  $\mathcal{B}(a_1^0 \rightarrow \tau^+ \tau^-)$  is 100%, the models above these lines are excluded. Our upper limits in the  $\gamma\tau^+\tau^-$  channel for lower  $a_1^0$  masses,  $2m_\tau < m_{a_1^0} < 7.5$  GeV (medium gray [red online] lines at the center of each plot), eliminate a significant fraction of models in this mass range (medium gray [red] points). Only very few models are challenged in the  $7.5 < m_{a_1^0} < 8.8$  GeV range (light gray [green] points and lines at the sides of scatter plots). For higher masses (black points and lines touching the plot axes), our discriminating power fades away as the backgrounds increase while the expected signal rate decreases

due to the phase space suppression. The nonsinglet fraction of  $a_1^0$  ( $\cos\theta_A$ ) increases with falling  $\tan\beta$  [2], though the net effect on  $g_d$ , and, therefore,  $\mathcal{B}(Y(1S) \rightarrow \gamma a_1^0)$ , is to decrease. At the same time,  $a_1^0$  coupling to up-type fermions,  $g_u \propto \cos\theta_A/\tan\beta$ , increases, lowering  $\mathcal{B}(a_1^0 \rightarrow \tau^+ \tau^-)$ . Thus, models with small  $\tan\beta$  values are less constrained by our data.

Since  $\mathcal{B}(a_1^0 \rightarrow \mu^+ \mu^-)$  is not expected to be large above the  $a_1^0 \rightarrow s\bar{s}$  threshold ( $\sim 1$  GeV), we did not transfer our limits on  $\mathcal{B}(Y(1S) \rightarrow \gamma a_1^0)\mathcal{B}(a_1^0 \rightarrow \mu^+ \mu^-)$  to Fig. 4, where NMSSM model calculations of  $\mathcal{B}(Y(1S) \rightarrow \gamma a_1^0)$  below the  $\tau^+ \tau^-$  threshold (blue points) were performed only for  $m_{a_1^0} > 1$  GeV. Our limits below this mass value constrain NMSSM scenarios. Of particular interest is our upper limit for  $m_{a_1^0} = 214.3$  MeV, i.e., the  $\mu^+ \mu^-$  mass of  $3 \Sigma^+ \rightarrow p\mu^+ \mu^-$  events observed by the HyperCP experiment [4]. The fit to our data (see Fig. 5) gives  $7.0^{+5.3}_{-4.3}$  events at this mass and leads to an upper limit of  $\mathcal{B}(Y(1S) \rightarrow \gamma a_1^0) < 2.3 \times 10^{-6}$  at 90% C.L. He, Tandean, and Valencia showed that they could explain the HyperCP events with the  $a_1^0$  hypothesis and still be consistent with the constraints from  $K \rightarrow \pi\mu^+ \mu^-$  experiments [5]. In their calculations, they used  $g_d^2 = 0.12$ , while our upper limit translates into  $g_d^2 < 0.026$  (using  $\mathcal{C} = 0.5$  [3]), which calls for reevaluation of the  $a_1^0$  hypothesis for the HyperCP events.

In summary, we have obtained meaningful upper limits on  $\mathcal{B}(Y(1S) \rightarrow \gamma a_1^0) \times \mathcal{B}(a_1^0 \rightarrow \tau^+ \tau^-)$  and  $\mathcal{B}(Y(1S) \rightarrow \gamma a_1^0) \times \mathcal{B}(a_1^0 \rightarrow \mu^+ \mu^-)$ . Our limits on  $\gamma\tau^+\tau^-$  are almost 2 orders of magnitude more stringent than those from ARGUS and eliminate a large portion of previously unconstrained parameter space in NMSSM models. Our limits on

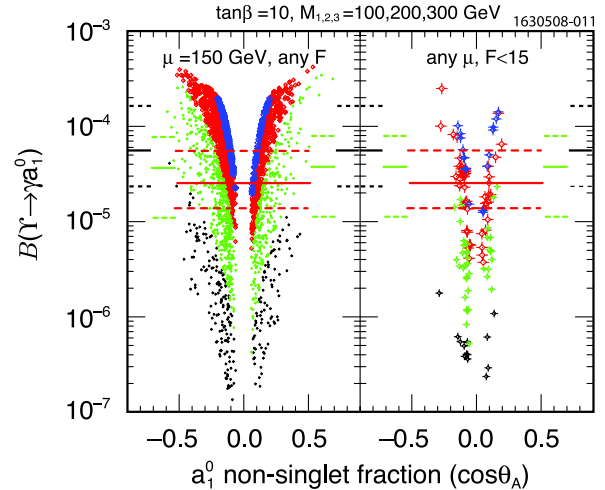


FIG. 4 (color online). Comparison of CLEO upper limits on  $\mathcal{B}(Y(1S) \rightarrow \gamma a_1^0) \times \mathcal{B}(a_1^0 \rightarrow \tau^+ \tau^-)$  (solid and dashed lines) to the NMSSM predictions by Dermisek, Gunion, McElrath (points) (figure modified from Fig. 1 of [2]). See the text for explanations.



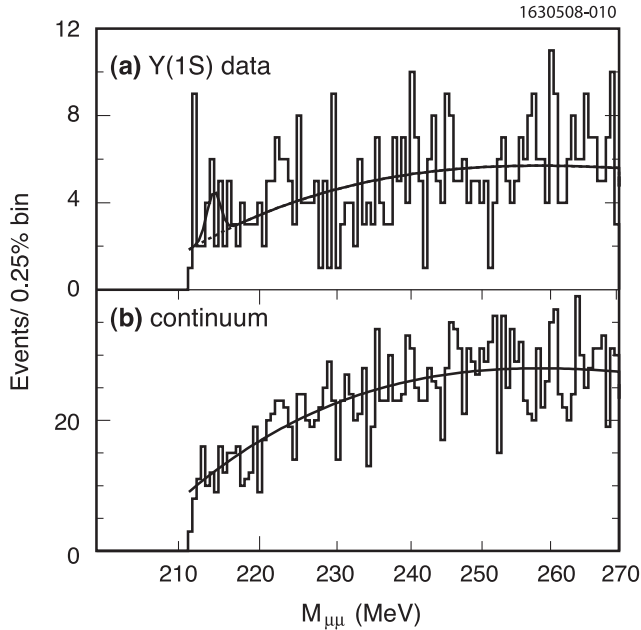


FIG. 5. A fit of a peak at a dimuon mass of 214.3 MeV with fixed width at the expected mass resolution, on top of cubic polynomial to our  $\gamma\mu^+\mu^-$  data obtained at the Y(1S) center-of-mass energy (a). The polynomial describing the continuum backgrounds was simultaneously constrained by the data collected at and near the Y(4S) resonance (b).

$\gamma\mu^+\mu^-$  challenge models with  $a_1^0$  mass below  $s\bar{s}$  threshold and the  $a_1^0$  interpretation of HyperCP  $\Sigma^+ \rightarrow p\mu^+\mu^-$  events. Our limits are applicable to any light scalar or pseudo-scalar boson, which arises in various extensions of Standard Model.

We gratefully acknowledge the effort of the CESR staff in providing us with excellent luminosity and running conditions. This work was supported by the A.P. Sloan Foundation, the National Science Foundation, the U.S. Department of Energy, the Natural Sciences and Engineering Research Council of Canada, and the U.K. Science and Technology Facilities Council. We thank Radovan Dermisek, Jack Gunion, Michelangelo Mangano, German Valencia, and Miquel Sanchis-Lozano for useful discussions of NMSSM models.

- 
- [1] R. Barate *et al.*, Phys. Lett. B **565**, 61 (2003).
  - [2] R. Dermisek, J. F. Gunion, and B. McElrath, Phys. Rev. D **76**, 051105(R) (2007).
  - [3] M. L. Mangano and P. Nason, Mod. Phys. Lett. A **22**, 1373 (2007).
  - [4] H. Park *et al.* (HyperCP), Phys. Rev. Lett. **94**, 021801 (2005).
  - [5] X. G. He, J. Tandean, and G. Valencia, Phys. Rev. Lett. **98**, 081802 (2007). The  $g_d$  coupling is denoted as  $l_d$  is this reference.
  - [6] Y. Kubota *et al.* (CLEO), Nucl. Instrum. Methods Phys. Res., Sect. A **320**, 66 (1992); D. Peterson *et al.*, *ibid.* **478**, 142 (2002); M. Artuso *et al.*, *ibid.* **554**, 147 (2005).
  - [7] E. Fullana and M. A. Sanchis-Lozano, Phys. Lett. B **653**, 67 (2007).
  - [8] D. Besson *et al.* (CLEO), Phys. Rev. Lett. **98**, 052002 (2007).
  - [9] Z. Was and M. Worek, Acta Phys. Pol. B **33**, 1875 (2002) [arXiv:hep-ph/0202007].
  - [10] T. Skwarnicki, Ph.D. Thesis, Cracow Institute of Nuclear Physics [Institution Report No. DESY-F31-86-02, 1986].
  - [11] H. Albrecht *et al.* (ARGUS), Phys. Lett. B **154**, 452 (1985).